Bottom up layer-by layer assembling of antibacterial freestanding nanobiocomposite films

Antonio Francesko[†], *Kristina Ivanova*[†], *Javier Hoyo*[†], *Sílvia Pérez-Rafael*[†], *Petya Petkova*[†], *Margarida M Fernandes*[†], *Thomas Heinze*[‡], *Ernest Mendoza*[§], *and Tzanko Tzanov*[*,†]

† Grup de Biotecnologia Molecular i Industrial, Department of Chemical Engineering, Universitat Politècnica de Catalunya, Rambla Sant Nebridi 22, Terrassa 08222, Spain. E-mail: tzanko.tzanov@upc.edu

‡ Center of Excellence for Polysaccharide Research, Institute of Organic Chemistry and Macromolecular Chemistry, Friedrich Schiller University of Jena, Humboldtstraße 10, Jena 07743, Germany

§ Grup de Nanomaterials Aplicats, Centre de Recerca en Nanoenginyeria, Universitat Politècnica de Catalunya, c/ Pascual i Vila 15, Barcelona 08028, Spain

[*] Corresponding author

KEYWORDS: chitosan, aminocellulose, hyaluronic acid, biopolymer-capped silver nanoparticles, layer-by-layer, freestanding antimicrobial films

ABSTRACT

In this study, freestanding nanobiocomposite films were obtained by the sequential deposition of biopolymer-capped silver nanoparticles (AgNPs) and hyaluronic acid (HA). At first, dispersions of AgNPs decorated with chitosan (CS) or aminocellulose (AC) were synthesized by applying high intensity ultrasound. These polycationic nanoentities were layer-by-layer assembled with the HA polyanion to generate stable 3D supramolecular constructs, where the biopolymer-capped AgNPs play the dual role of active agent and structural element. SEM images of the assemblies–revealed gradual increase of thickness with the number of deposited bilayers. The composites of ≥50 bilayers were safe to human cells and demonstrated 100% antibacterial activity against *Staphylococcus aureus* and *Escherichia coli*. Moreover, the films containing CSAgNPs brought about the total prevention of biofilm formation reducing the cells surface adherence by up to 6 logs. Such nanobiocomposites could serve as an effective barrier to control bacterial growth on injured skin, burns and chronic wounds.

INTRODUCTION

Composite materials combine multiple components with different physicochemical characteristics, yielding hybrid structures with a broad range of functionalities and superior performance compared to their individual constituents. In recent years, important progress has been made in the field of biomaterial composites, which now have a major impact in the development of novel biocompatible materials.[1,2] Advances in nanobiocomposites fabrication, where one of the building phases shows nanometer range dimension, are of particular interest due to the unique properties of nanoparticles (NPs) imparting exceptional chemical, physical and biological characteristics to the composites.[3]

Layer-by-layer (LbL) assembling is one of the most rapidly growing technologies for generating 2D coatings and complex 3D biocomposite materials based on electrostatic interactions between oppositely charged compounds.[4,5] LbL assembly is also suitable for incorporation of one or several functional components including biological molecules and NPs into materials.[6,7] These components embedded between the layers can be subsequently released in a controlled manner from the multilayer construct.[7–9]

In case of a low number of deposited layers, usually less than 20, the coating must be anchored on the supporting substrate that maintains its mechanical properties and shape, behaving as an integrated macroscopic system.[10,11] By contrast, building higher number of layers allows for detaching the multilayer system from the substrate and use it as a 3D freestanding construct. In such case, the embedded components and the number of layers define the mechanical properties and functionality of these sequentially nano-built macro-structures, without the need for a supporting substrate. Freestanding scaffolds for tissue

engineering have been successfully developed following this rationale,[12–16] whereas stand-alone LbL nanobiocomposite films with antimicrobial activity have been scarcely reported.[17] Actually, the development of easily detachable LbL films incorporating nano-sized compounds as active and/or constructive elements is a challenging task and frequently requires post-fabrication treatments.[18–20]

In this work, we fabricated hybrid films incorporating aminocellulose (AC) or chitosan (CS)-capped silver nanoparticles (AgNPs). The goal of assembling biopolymers and antibacterial inorganic AgNPs is to fabricate safe by design biocompatible films to inhibit the growth and adhesion of Gram-negative and Gram-positive bacteria, limiting the risk of infections in burn, surgical wound, or injury.[21,22] Silver was chosen as a largely recognized efficient antimicrobial agent, especially in its nano form.[23–25] AgNPs, however, present some drawbacks, such as nanotoxicity, complicated fabrication and poor colloidal stability.[26] By contrast, we employed a technologically simple, relatively fast and ecologically acceptable methodology for simultaneous synthesis and capping of AgNPs with biopolymers. Our approach yields stable, highly concentrated and biocompatible hybrid biopolymer-AgNPs dispersions using AC or CS as reducing and stabilizing agents.[27,28] The obtained cationic biopolymer-AgNPs were further incorporated into multilayer assemblies with hyaluronic acid (HA) which were easily detached as freestanding films from the underlying silicone template without the need of any post-processing steps. The engineered films were tested for their ability to inhibit the growth and biofilm formation of the common skin and soft tissue pathogens *Staphylococcus aureus* (*S. aureus*) and *Escherichia coli* (*E. coli*), without affecting the human skin cells.[29,30]

MATERIALS AND METHODS

Reagents

Medical grade CS from *Agaricus bisporus* (Mw ~15 kDa and DDA = 87%) provided by Kitozyme (Belgium) and the cellulose derivative, 6-deoxy-6-(ω-aminoethyl) aminocellulose (Mw ~15 kDa) synthesized from microcrystalline cellulose (Fluka, Avicel PH-101) via a tosyl cellulose intermediate,[28,31] were used as reducing and capping agents in the biopolymer-AgNPs synthesis. Sodium salt of hyaluronic acid (HA, Mw ~ 750 kDa) was purchased from Lifecore Biomedical (USA) and utilized as a polyanion. $AgNO_3$, (3-aminopropyl)triethoxysilane (APTES), acetic acid, sodium chloride (NaCl), hydrochloric acid (HCl), sodium hydroxide (NaOH), sodium dodecyl sulfate (SDS), poly(ethyleneimine) (PEI), acetone, ethanol and isopropanol of analytical grade were purchased from Sigma-Aldrich (Spain). Antimicrobial tests were carried out with Gram-positive *S. aureus* ATCC® 25923™ and Gram-negative *E. coli* ATCC® 25922™ bacteria. Nutrient broth (NB) from Sharlab (Spain) was used as growth medium in all antibacterial tests, whereas tryptic soy broth (TSB) obtained from Sigma-Aldrich (Spain), was employed in the biofilm inhibition tests. Baird-Parker and Coliform selective agars for culturing and enumeration of *S. aureus* and *E. coli*, respectively, were also purchased from Sigma-Aldrich (Spain). Live/Dead® BacLight™ kit (Molecular probes L7012) and AlamarBlue™ Cell Viability Reagent were obtained from Invitrogen, Life Technologies Corporation (Spain). Polydimethyl/vinylmethyl siloxane (silicone) strips (ASTM D 1418) were provided by Degania Silicone Ltd. (Israel).

Synthesis and characterization of biopolymer-capped Ag NPs

Concentrated dispersions of biopolymer-AgNPs (ACAgNPs and CSAgNPs) were synthesized according to a previously described procedure.[27] Briefly, 20 mL of aqueous $AgNO_3$ (2 mg mL^{-1}) were mixed with 30 mL of 1% (w/v) aqueous AC solution or 1% (w/v) CS solution prepared in 1% acetic acid. The pH was adjusted to 5.5 with 3 M NaOH and the mixtures were sonicated during 3 h with Ti-horn 20 kHz (Sonics and Materials VC750, USA). The reaction temperature of 60 ºC was maintained with a thermostatic bath. The US parameters were determined calorimetrically as follows: intensity 17.30 W cm^{-2}, density 0.43 W cm^{-3} and power 21.5 W.

The spectra of ACAgNPs and CSAgNPs were collected in the 300-600 nm range, recording the absorbance at a 2 nm step, with a microplate reader Infinite M200 (Tecan, Austria). The size, polydispersity index and ζ-potential of the NPs were determined using a Zetasizer Nano ZS (Malvern Instruments Inc., UK). Then, images of the NPs hybrids were acquired with a Zeiss Neon FIB microscope (Carl Zeiss, Germany) operating in scanning transmission electron microscopy (STEM) mode at 30 kV acceleration voltage. Due to the high NPs concentrations, the dispersions were diluted 100-fold and 20 µL aliquots were drop-casted on the holey carbon grids.

Fabrication of multilayer antibacterial films

Multilayer films were fabricated on silicone strips previously washed with 0.5% (w/v) SDS, distilled water and ethanol. After washings, the silicone surface was amino-functionalized using APTES to allow the deposition of first HA (polyanion) layer via the

electrostatic interactions between the carboxyl groups of HA and the amino groups on the surface. The APTES pretreatment of silicone was carried out according to a previously described procedure.[32] Cationic ACAgNPs or CSAgNPs dispersions and anionic solution of HA, with final concentrations of 0.5 mg mL^{-1} were prepared in 0.15 M NaCl. Aqueous solutions of 1 M HCl and 1 M NaOH were used to adjust the pH of all polyelectrolytes to 5.5. Multi-vessel automated dip coater (KSV NIMA, Finland) was used for automatic alternate deposition on the silicone strips of 10, 50, 100 and 200 bilayers of HA and ACAgNPs or CSAgNPs. Each adsorption step lasted 10 min, followed by a 10 min rinsing in 0.15 M NaCl, pH 5.5. The materials composed of 10 bilayers were considered coatings, whereas those of 50, 100 and 200 bilayers were called films. The biocomposites were designated as HA-ACAgNPs when ACAgNPs hybrid was used as a polycation and HA-CSAgNPs in case of CSAgNPs hybrid. The samples were further thoroughly washed with distilled water and after drying at room temperature, the films were detached from the silicone strips and subjected to specific analyses.

Monitoring of multilayer assembly with quartz crystal microbalance with dissipation

The LbL build-up of HA and ACAgNPs or CSAgNPs was followed *in situ* with a quartz crystal microbalance with dissipation (QCM-D, E4 system, Q-Sense, Sweden). The deposition was performed onto gold coated sensor crystals QSX 301 (QSense, Sweden) at 22 ºC and at a constant flow rate (80 µL min^{-1}). Prior LbL assembly, the crystals were cleaned successively by US bath in acetone, ethanol and isopropanol for 10 min at 40 ºC. Thereafter, the crystals were incubated overnight at room temperature in 1

mg mL^{-1} PEI solution for amino functionalization of their surface. The modified sensors were washed, dried under nitrogen stream and placed in the QCM-D flow chambers.

The baseline was carried with 0.15 M NaCl, pH 5.5. The multilayer assembly of ACAgNPs or CSAgNPs and HA was repeated 5 times to obtain 5 bilayers on the amino-functionalized crystals. To simplify the data interpretation, only the normalized frequency ($\Delta f/\nu$) and dissipation (ΔD) shifts as a function of time of one representative sample per experimental group (5^{th} harmonic) is shown.

Characterization of the multilayer films

Attenuated total reflection Fourier transform infrared spectroscopy (ATR-FTIR) was used to characterize the multilayer materials. For this purpose, the AC- and CS-based coatings of 10 bilayers were analyzed in a Spectrum 100 FT-IR spectrometer (Perkin Elmer, USA). The spectra were obtained between 4000-625 cm^{-1} performing 64 scans at 4 cm^{-1} resolution. Prior to the FTIR analysis the specimens were dried under nitrogen until no water was detected during the analyses.

The dry thickness of the LbL coatings on the silicone support and the films were further investigated by scanning electron microscopy (SEM) (JSM 5610, JEOL Ltd, Japan). The cross sections of the film were obtained by a single cut of the dried under nitrogen specimens. The surface morphology of the films was studied by field emission SEM (FESEM) JEOL J-7100 with Energy-dispersive X-ray spectroscopy (EDS) detector. Atomic force microscopy (AFM) topographic images of the nanobiocomposites were acquired in an air tapping mode using a Multimode AFM controlled by Nanoscope IV

electronics (Veeco, Santa Barbara, CA) under ambient conditions. Triangular AFM probes with silicon nitride cantilevers and silicon tips were used (SNL-10, Bruker) (nominal spring constant of 0.35 N/m and a resonant frequency of 50 kHz). Images were acquired at 1 Hz line frequency and at minimum vertical force to reduce sample damage. The surface roughness was calculated from the acquired images with Nanoscope Analysis 1.5 software.

The total amount and the cumulative release of silver from the freestanding multilayered films (100 and 200 bilayers) were determined with an inductively coupled plasma mass spectrometry (ICP-MS) calibrated by internal standard with ^{115}In and a standard curve of ^{107}Ag. For silver quantification the films were cut (1 x 1 cm^2) and digested with 20 % HNO_3. The cumulative release of silver ions from the films was studied in phosphate-buffered saline (PBS) over seven days. The films (1 x 1 cm^2) were incubated in 40 mL 0.01 M PBS, pH 7 at 37 ºC. At defined time intervals 1 mL of the solution was collected and acidified with HNO_3 before analysis with ICP-MS (PerkinElmer Ltd.).

Inhibition of bacteria growth

The potential of the multilayer coatings and films to inhibit the bacterial growth was assessed by a standard flask shake method (ASTM-E2149-01).[33] Single colonies isolated on tryptic soy agar plates by streaking technique were used in order to prepare *S. aureus* and *E. coli* cultures. The cultures were then inoculated overnight in 5 mL sterile NB and incubated at 37 ºC and 110 rpm. The inoculated bacteria cultures were diluted in sterile 0.3 mM potassium dihydrogen phosphate, pH 7.2 (KH_2PO_4) until absorbance of 0.28 ±

0.01 at 475 nm was reached, which corresponds to 1.5 - 3.0 x 10^8 colony-forming unit (CFU) per mL. Thereafter, the silicone coated with 10 bilayers coatings and the films were cut in 1 x 1 cm^2 pieces that were incubated with 5 mL of bacterial suspension (final concentration 1.5 - 3.0 x 10^5 CFU mL^{-1}) at 37 ºC and 230 rpm for 1 h. The determination of the inoculum cell density of the suspensions was carried out by withdrawing part of the suspension before introducing the pieces and after 1 h in contact with them. The withdrawn suspensions were serially diluted in sterile buffer solution, plated on a Baird-Parker agar or Coliform agar and incubated at 37 ºC for 24 h to determine the number of viable bacteria. The antibacterial activity is reported in terms of percentage of bacterial reduction calculated as the ratio between the number of bacteria before and after the contact with the samples using the following equation:

$$\text{Reduction of viable bacteria (\%)} = ((A-B) / A) \times 100$$

where A and B are the average number of viable bacterial cells (i.e. counted CFU) before and after the contact with the multilayer materials, respectively.

Inhibition of bacterial biofilms

The ability of the developed multilayer materials to counteract pathogenic biofilm formation of *S. aureus* and *E. coli* was studied by fluorescence microscopy and viability counts. Overnight-grown cultures of *S. aureus* and *E. coli* were diluted in TSB to an optical density $(O.D.)_{600}$ = 0.01, corresponding to ~ 2 x 10^5 CFU mL^{-1}. The multilayer-coated silicone strips and films were cut into 1×1 cm^2 pieces and placed in a 24-well plate. Then, 1 mL of the bacterial suspension was inoculated in each well, and the plate

was incubated for 24 h at 37 ºC. The biofilms were washed with 1 mL 0.9% NaCl solution pH 6.5 three times and the biofilm growth on the materials was assessed measuring the fluorescence at 480/500 nm after 15 min staining with a mixture of green fluorescent Syto 9 and red-fluorescent Propidium iodide stains (1:1) of Live/Dead® BacLight™ kit.

S. aureus and *E. coli* biofilms grown for 24 h on the films were also quantitated by direct enumeration of the live bacteria. The non-attached cells were rinsed (3x) with 1 mL of sterile 0.9% NaCl, pH 6.5 and the samples were transferred into sterile tubes containing 2 mL 0.9% NaCl, pH 6.5. Then, the tubes were placed in an ultrasonic bath for 20 min and the viable counts were performed by plating bacterial suspension on selective agar plates.

Biocompatibility assessment

Human foreskin fibroblasts (ATCC®-CRL-4001™, BJ-5ta) and keratinocytes (HaCaT cell line) were used to assess the biocompatibility of the films. The cells were maintained in 4 parts Dulbecco's Modified Eagle's Medium (DMEM, ATCC) containing 4 mM of L-glutamine (ATCC), 4500 mg L^{-1} glucose, 1500 mg L^{-1} sodium bicarbonate and 1 mM sodium pyruvate, and 1 part of Medium 199 supplemented with 10% (v/v) of fetal bovine serum and 10 g mL^{-1} hygromycin B, at 37 °C in a humidified atmosphere with 5% CO_2. At pre-confluence, the cells were harvested using trypsin-EDTA (ATCC-30-2101, 0.25% (w/v) trypsin/0.53 mM EDTA solution in Hank's BSS without calcium or magnesium) and seeded at a density of 5.1 x 10^4 cells/well on a 24-well tissue culture treated polystyrene

plate (Nunc). After 24 h, the cells were washed twice with sterile PBS; the samples were placed in the wells and 1 mL of complete growth medium (DMEM) were added. The cells were incubated at 37°C for 1 and 7 days. At the end of these periods, the samples were removed, the growth media withdrawn and the cells were washed twice with PBS and stained for 4 h at 37°C with 100 μL 10% (v/v) AlamarBlue™ Cell Viability Reagent in DMEM. After that, the absorbance at 570 nm was measured, using 600 nm as a reference wavelength, in a microplate reader. The quantity of resorufin formed is directly proportional to the number of viable cells. Cells relative viability (%) was determined for each sample and compared with that of cells incubated only with culture medium. H_2O_2 (500 μM) was used as a positive control of cell death. Data are expressed as the mean of three measurements, with a standard deviation as a source of error.

RESULTS AND DISCUSSION

Synthesis of concentrated biopolymer-AgNPs dispersions

In our previous work, AgNPs capped with CS (CSAgNPs) were sonochemically synthesized in a 3-hours process at 60 ºC. Concentrated NPs suspension with more than 6 months stability was obtained.[27] For the purpose of the current study, NPs dispersions of both ACAgNPs and CSAgNPs were generated and used to construct supramolecular materials by LbL assembling. Besides of CS, the synthesis/stabilization approach for AgNPs production was extended to the application of another cationic polysaccharide under the same sonochemical processing conditions. The NPs formation was confirmed by UV-Vis spectroscopy displaying absorbance peaks of similar intensity at around 420 nm (Fig. 1) derived from the typical excitation of surface plasmon vibrations of Ag

atoms. The biopolymer-capped AgNPs were spherical in shape with size about 100 nm (Fig. 1, inset STEM images), low polydispersity index and high ζ-potential (Table S1). The absence of NPs complexes in STEM images further confirmed their high stability to aggregation. It is worthy to mention that some aggregation was expected to occur during drying the dispersions on the TEM grids.

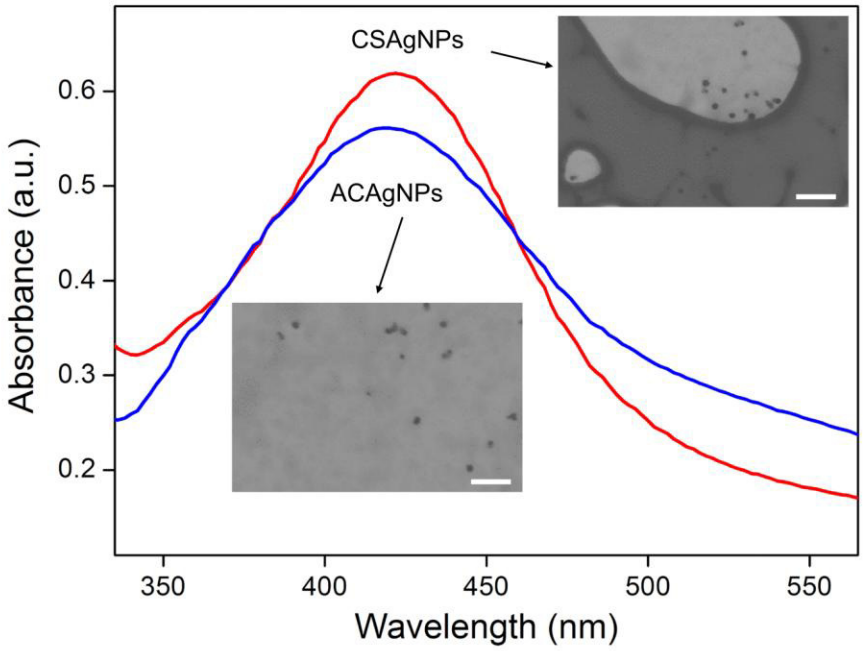

Figure 1. UV-vis spectra and STEM images of ACAgNPs and CSAgNPs dispersions synthesized under sonication during 3 h at 60 ºC. The scale bars correspond to 1000 nm.

In situ monitoring of the multilayer build-up

ACAgNPs and CSAgNPs with high positive charge density and large surface to volume ratio were further used as both building element and antibacterial active agent in the bottom up LbL fabrication of functional freestanding composite films. The films were

LbL assembled on template surfaces by the alternating deposition of positively charged CS- or AC-capped AgNPs and negatively charged hyaluronic acid (HA).

The LbL build-up of HA and ACAgNPs or CSAgNPs was assessed *in situ* with a QCM-D. The frequency (Δf_n) and dissipation (ΔD_n) changes obtained at the 5th overtone during layers assembling onto a PEI-functionalized gold crystal are shown in Fig. 2. The stepwise decrease in Δf_5 and increase of ΔD_5 after each deposition step confirmed the successful deposition of the anionic HA and cationic biopolymer-AgNPs in a LbL fashion. The changes in Δf_5 and ΔD_5 confirmed the effective interaction between building elements and suggested an exponential growth of the multilayer films comprising low- and high-Mw compounds.[11] Moreover, the washing of the weakly adsorbed compounds after each deposition step led to negligible changes in the Δf_5 and ΔD_5 values, indicating strong interaction between the biopolymer-AgNPs and HA and consequent formation of stable assemblies. Such behavior highlights the possibility of using small positively charged nano-sized entities as anchoring points for formation of stable multilayers that can be easily detached from the substrate template to form freestanding films. Remarkably, the variations in Δf_5 and ΔD_5 are more pronounced in the constructs where CSAgNPs are present, which is correlated with the formation of thicker layers. CSAgNPs possess enhanced cationic character in comparison to ACAgNPs owing to the higher pKa of CS (pKa ~ 6.5)[34] vs AC (pKa ~ 5.2)[35] and therefore induce stronger electrostatic interactions with HA, favoring the coating build-up. The continuous increase in the ΔD_5 on the other hand indicated that the assembled multilayers are soft and demonstrate damping properties similar to other polymeric systems.

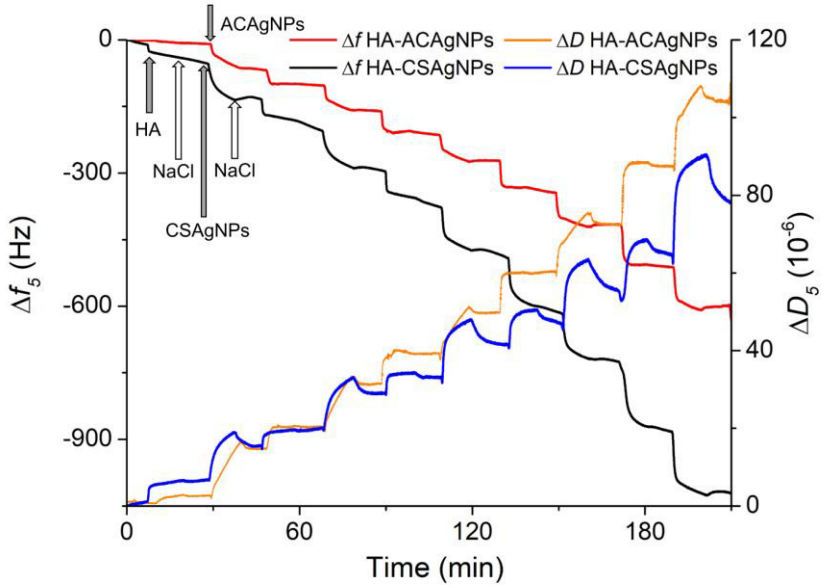

Figure 2. QCM-D monitoring of normalized frequency (Δf_5) and dissipation (ΔD_5) obtained at 5th overtone as a function of time during the build-up of 5 HA-CSAgNPs and HA-ACAgNPs bilayers.

Fabrication and characterization of the NPs-containing multilayer nanobiocomposites

ACAgNPs and CSAgNPs (as polycations) were sequentially deposited on the surface of APTES-functionalized silicone strips using HA as an alternate polyanion. Unlike the 10 bilayers, the 50 and especially the 100 and 200 bilayer films, could be easily detached from the silicone substrate, without any post-treatment, and handled for further analyses (Fig. 3III).

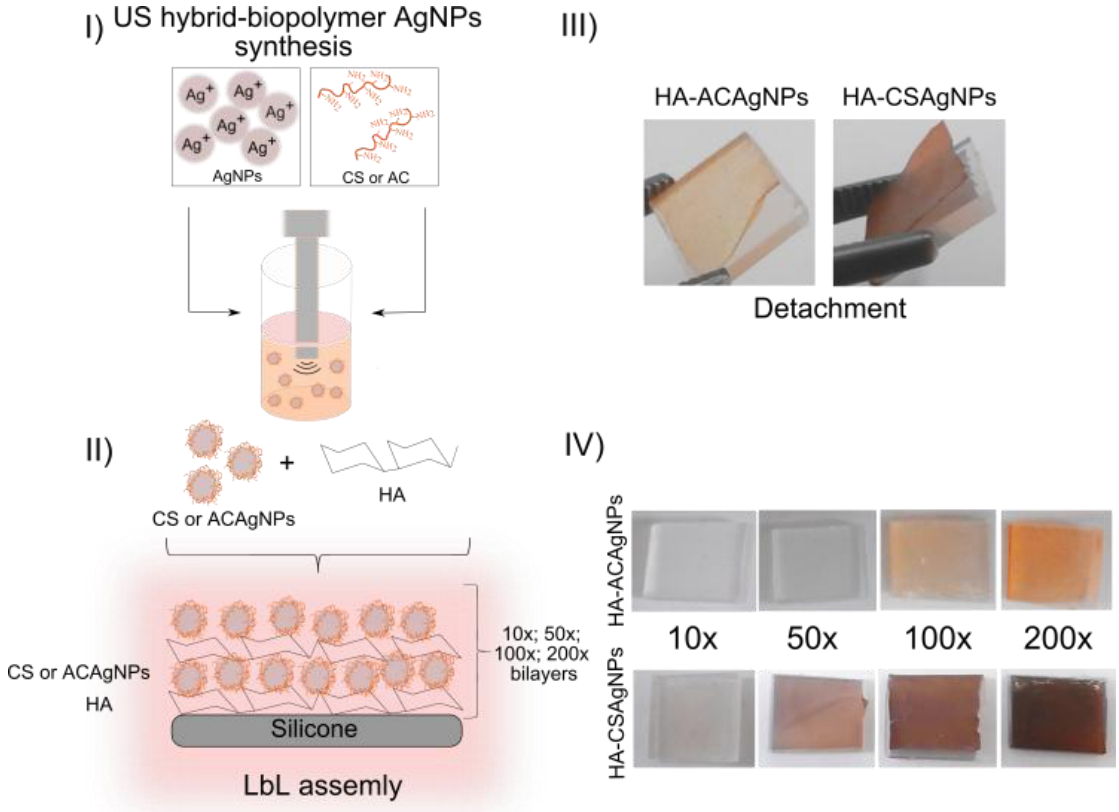

Figure 3. Fabrication of freestanding nanobiocomposite films from HA-ACAgNPs or HA-CSAgNPs (I and II), and their detachment from silicone (III). AgNPs are oversized in the scheme to illustrate the concept for the multilayer build-up. Photographs of the coatings/freestanding films are also shown (IV).

Since it was not expected that the increasing number of layers would influence the infrared spectra of the coatings,[7] the ATR-FTIR was performed only on the 10 bilayer constructs. The deposition of HA-ACAgNPs and HA-CSAgNPs was evidenced by the appearance of several new bands compared to the aminated silicone control surface (Fig. 4).

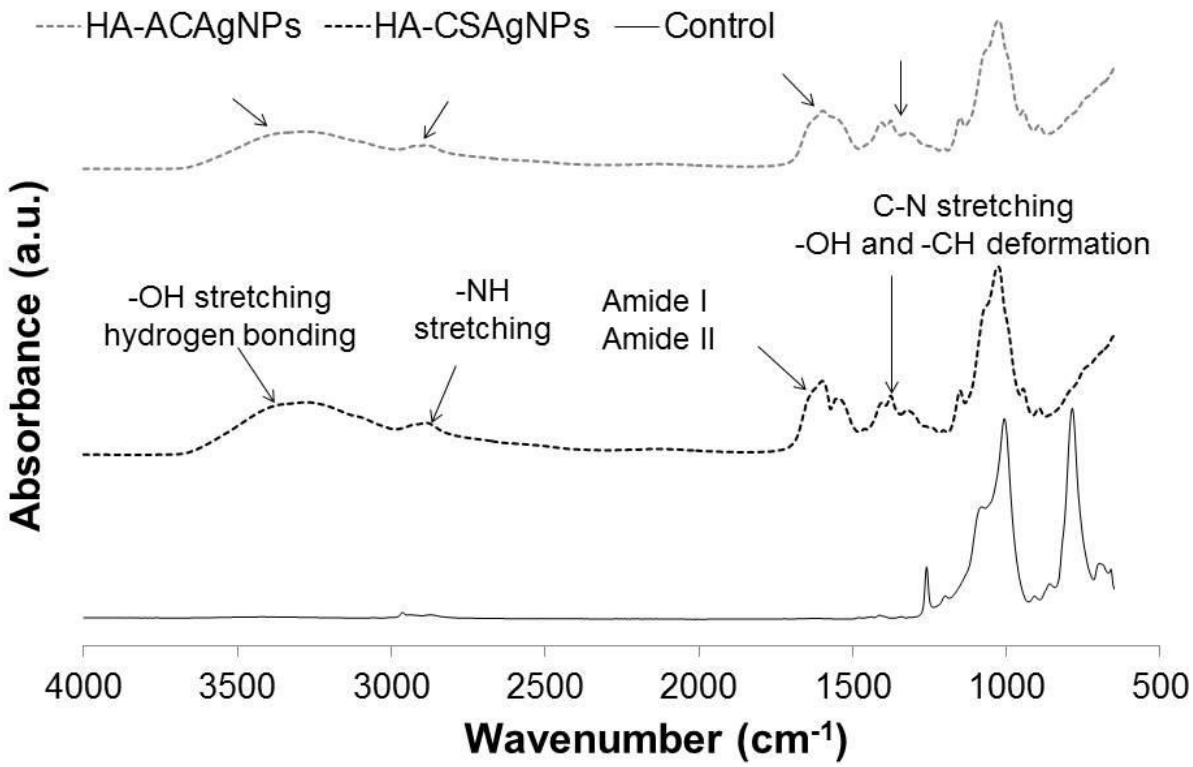

Figure 4. ATR-FTIR spectra of APTES-treated silicone control and the silicones coated with 10 bilayers of HA-ACAgNPs (grey dashed line) and HA-CSAgNPs (black dashed line).

These peaks were related to the presence of cationic polyelectrolytes (AC or CS) and the polyanion (HA), as well as the interactions between them. The peaks at around 2900 and 1346 cm^{-1} come from the stretching vibrations (-NH) in amino groups of AC or CS, while the peak at 1420 cm^{-1} belongs to both hydroxyl (-OH) and alkyl ($-CH_2$) group deformations in the cyclic structures of the three polysaccharides (AC, CS and HA). These peaks confirmed that the multilayer structures comprised both cationic and anionic polyelectrolytes. The interaction of the oppositely charged components in the coatings led to the appearance of the band at 3500 cm^{-1}, owing to the stretching of hydroxyl groups (-OH) involved in hydrogen bonding between the carboxylic groups from HA and the

amine groups in AC or CS.[36] Such interaction was corroborated by the appearance of the bands at 1627 and 1570 cm^{-1}, assigned to the typical amide I and amide II, respectively.

The SEM images taken at the cross-section of the LbL materials showed that 10 alternate depositions (coatings) were not sufficient to obtain an even coverage of the silicone surface, regardless of the choice of the polycation (AC or CS) (Fig. 5). In these cases a dry thicknesses of ~1 μm was measured on isolated islets, emerged from the coated silicone surface. These islets grow in diameter with increasing number of deposited layers and eventually coalesce into continuous coatings in the so-called "second stage" of the build-up process, usually above 10-20 bilayers.[37]

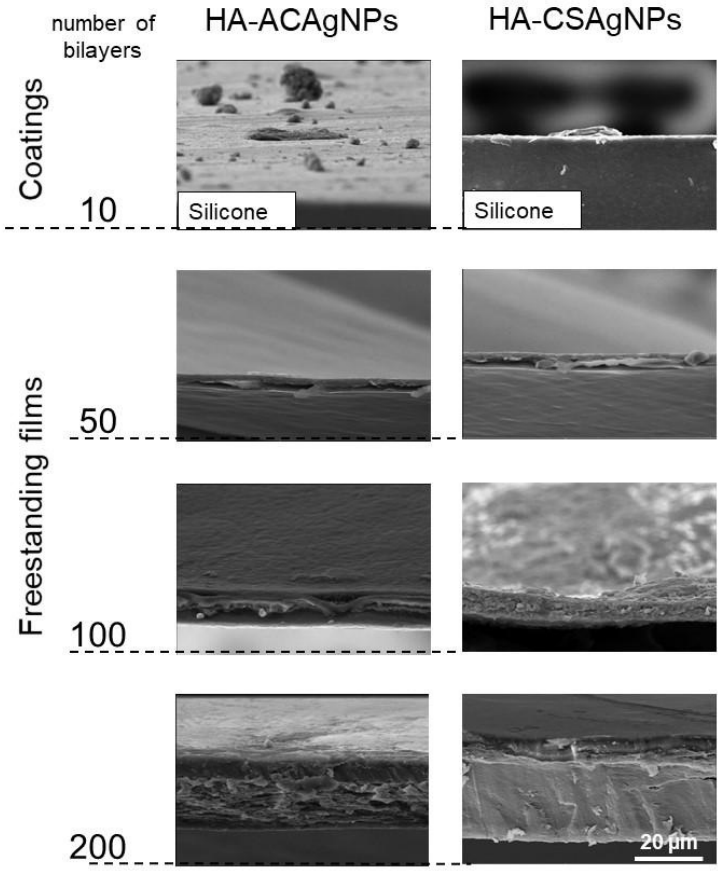

Figure 5. SEM micrographs of cross-sections of the representative coatings and freestanding LbL nanobiocomposite films comprising different number of bilayers: HA-ACAgNPs (left column), HA-CSAgNPs (right column). Magnification x5000.

For the nanobiocomposite constructs with ≥50 bilayers, a reasonably homogeneous deposition of the last layer was revealed by SEM. In fact, the dry thickness of the AgNPs-containing films gradually increased with the increasing number of deposited bilayers. The thickest films were expectedly those comprised of 200 bilayers (Table 1 and Fig. 5), especially valid for the films containing CSAgNPs.

Table 1. Average thickness of HA-ACAgNPs and HA-CSAgNPs multilayer coatings and films

Coating/Membrane	Nº of bilayers	Thickness
HA-ACAgNPs	10	~1.1 μm
	50	2.9 μm
	100	8.5 μm
	200	16.1 μm
HA-CSAgNPs	10	~1.2 μm
	50	5.8 μm
	100	12.5 μm

	200	24.2 μm

The nanobiocomposite constructs with 100 and 200 bilayers displayed a homogeneous surface topography (Fig. 6 and Fig. S1) in agreement with previous SEM observations (Fig. 5). In contrast to the HA-ACAgNPs films, silver NPs of ≈100 nm were clearly observed on the surface of CS-based constructs, further confirmed by the EDS analysis (Fig. S2). The root mean square roughness (R_q) obtained from the AFM images revealed a decrease in the surface irregularities with the deposition of more HA/biopolymer AgNPs bilayers (Table S2). Previous studies in our group showed the same tendency for multilayer assembled with cationic nano-sized entities.[7]

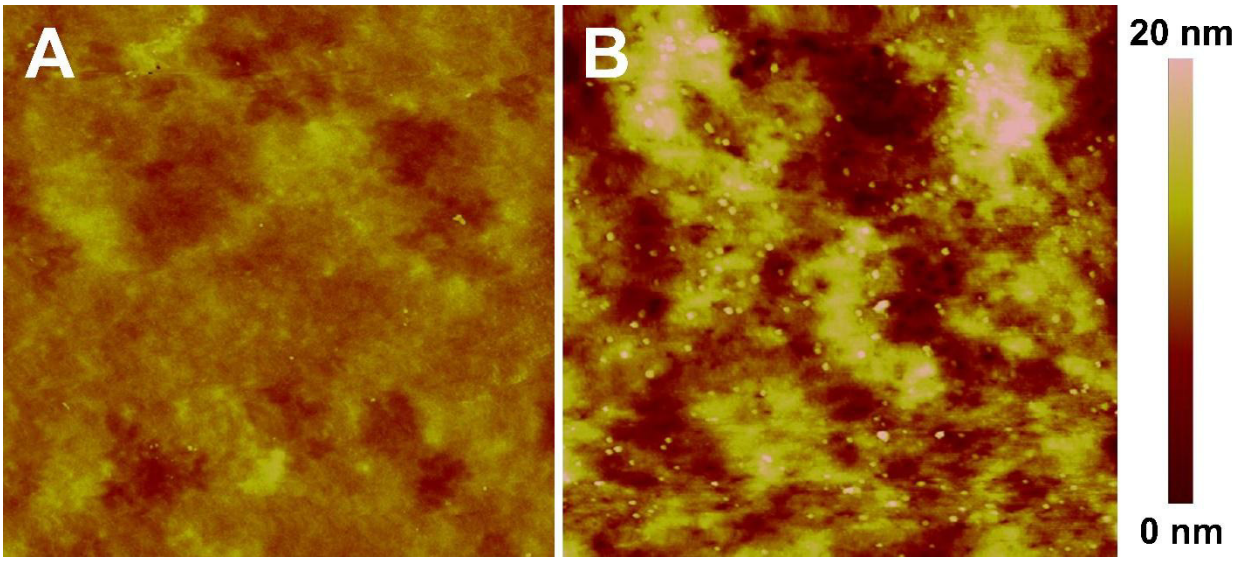

Figure 6. Topographic AFM images (5 x 5 μm) of the freestanding LbL nanobiocomposite films comprising 200 bilayers: A) HA-ACAgNPs and B) HA-CSAgNPs.

ICP-MS measurements quantified the total amount and the release of silver from the freestanding films. The 100 and 200 bilayers LbL films comprising CSAgNPs contain more silver (0.19 % and 0.44 % (w/w)) than those with ACAgNPs (0.01 % and 0.02 % (w/w)), respectively. The strong electrostatic interactions of CSAgNPs with anionic HA results in more mass deposition, including AgNPs and HA, and formation of thicker films, as confirmed by QCM-D (Fig. 2) and SEM (Fig. 5). Nevertheless, very similar release profiles were observed in each group of studied films, e.g. CS or AC containing, showing an initial burst release over the first 24 h followed by a sustained release during a week (Fig. 7). After 7 days of incubation, higher silver release, 371 and 278 ppb, was detected for HA-CSAgNPs films with 200 layers and 100 layers, respectively. On the other hand, only 158 and 60 ppb of silver were released from HA-ACAgNPs comprised of respectively 200 and 100 bilayers. Such noticeable difference in the amount of silver released from these films over 7 days is related to the total load of ACAgNPs and CSAgNPs in each specimen. The sustained release profiles of antibacterial silver make the LbL films suitable for limiting the growth and spread of bacterial pathogens on non-living and living surfaces.

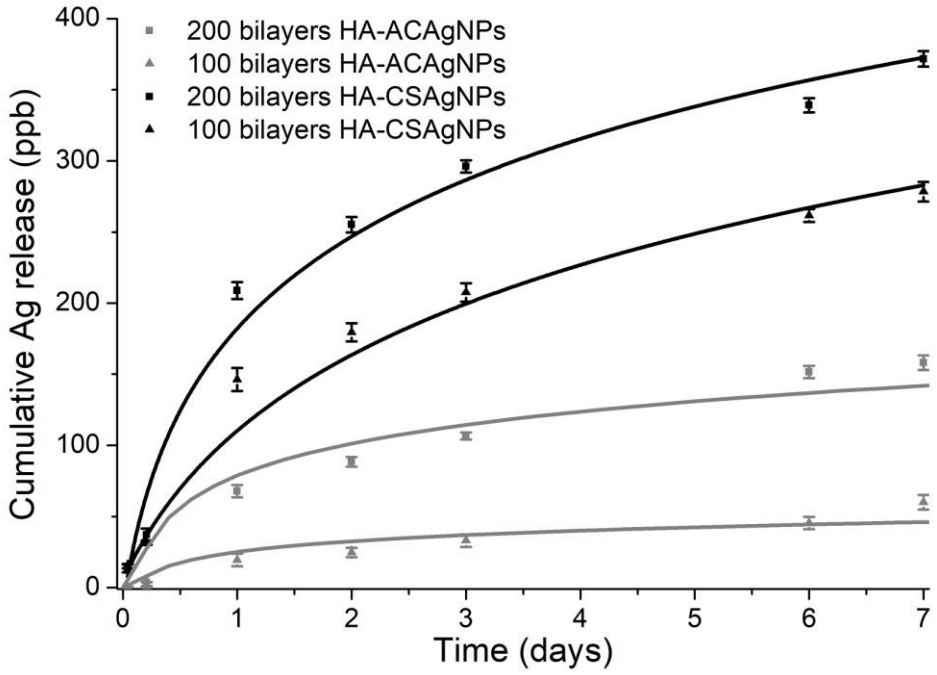

Figure 7. Cumulative silver release from HA-ACAgNPs and HA-CSAgNPs films.

Antibacterial effect

Since AgNPs are widely known as efficient antibacterial agents against both Gram-positive and Gram-negative bacteria, the antibacterial efficiency of the LbL coatings and films was evaluated against the medically relevant representative of skin infections - *S. aureus* and *E. coli*.[29,30] All LbL films, i.e. HA-ACAgNPs or HA-CSAgNPs with ≥ 50 bilayers, displayed full kill (100% viability reduction) for both bacterial strains, whereas the 10 bilayers coatings were not as efficient apparently due to the lower concentration of the antibacterial agent (Fig. 8 and Fig. S3).

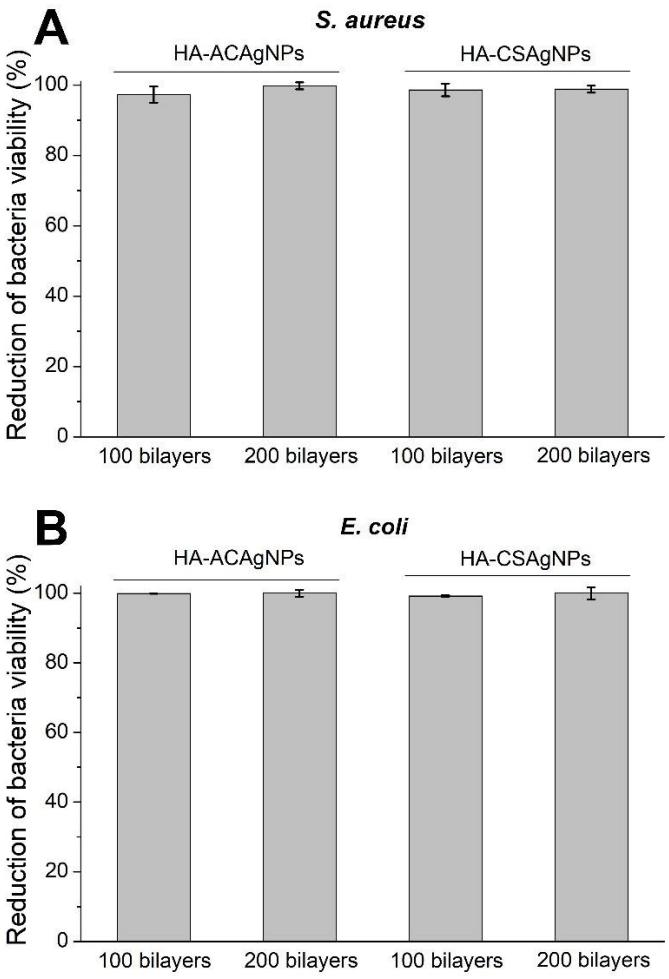

Figure 8. Reduction of *S. aureus* and *E. coli* viability using HA-ACAgNPs and HA-CSAgNPs films comprising 100 and 200 bilayers.

The adhesion of *S. aureus* and *E. coli* and subsequent establishment of bacterial biofilms on the films was further assessed by fluorescence microscopy and viable cell counts. The nanobiocomposites inhibited the biofilm growth to a different extent as compared to pristine silicone, on which the individual cells formed robust sessile bacterial communities (Fig. 9). Although the LbL coatings with 100 bilayers of HA-ACAgNPs or HA-CSAgNPs significantly reduced *S. aureus* and *E. coli* biofilms compared to the

pristine silicone, their surface was still colonized with bacterial clusters. Further increase in the number of bilayers to 200 considerably improved the antibiofilm activity of the films. The build-up of 200 bilayers brought about the total prevention of the *S. aureus* and *E. coli* biofilm formation on HA-CSAgNPs, reducing the viable cells on the surface by 7 logs and 6 logs, respectively (Fig. S4). However, 200 bilayers freestanding films with ACAgNPs demonstrated even lower antibiofilm activity towards Gram-negative *E. coli*, as more bacterial clusters on the surface were observed (Fig. 9). These findings were further confirmed by enumeration of the surface attached viable *E. coli* cells (Fig. S4). In general, Gram-positive bacteria are considered more resistant to AgNPs than Gram-negative ones due to the thick peptidoglycan layer in their cell wall, which serves as a protective barrier and limits the NPs uptake.[38] However, capping AgNPs with cationic biopolymers promotes the interaction with the negatively charged bacterial cells, and together with Ag synergistically increases the bactericidal potential of the hybrids. We have already shown the ability of cationic AC and thiolated CS NPs to disrupt bacterial membrane, leading to cells death at lower concentrations.[39] Herein, the films composed of CS or AC capped AgNPs affected in a similar fashion the growth of free-floating (planktonic) *S. aureus* and *E. coli* cells (Fig. 8). By contrast, their antibiofilm potential was higher towards *S. aureus*, which may be attributed to the presence of HA as already observed in previous works.[5,40] However, bacterial attachment and biofilm formation on surfaces is a more complex processes governed by a large number of factors including surface charge, hydrophobicity and roughness.[41] Smooth top layers, such as those of the films (Fig. 5 and 6, Table S2), are known to decrease the non-specific protein attachment and bacterial colonization.[42–44] Indeed, creating a smooth nanostructured surface was our

goal to prevent the bacterial adhesion, since most of the natural anti-biofilm surfaces reported to date are known to possess well-organized micro/nanoscale surface patterns at a "sub-bacterial" scale, i.e. < 1 μm in length.[44,45] Other strategies to control bacterial colonization range from anti-adhesive surfaces that aim at preventing the host proteins adherence and repelling bacteria,[46] to antibacterial materials able to kill pathogens either upon release of the biocide or at contact with bacteria cells.[47,48] The smooth membrane surface, the controlled antimicrobial silver release, and the presence of antifouling HA and hybrid-biopolymer NPs in the multilayers synergistically improve the antibacterial/antibiofilm potential of the engineered nanobiocomposite films.

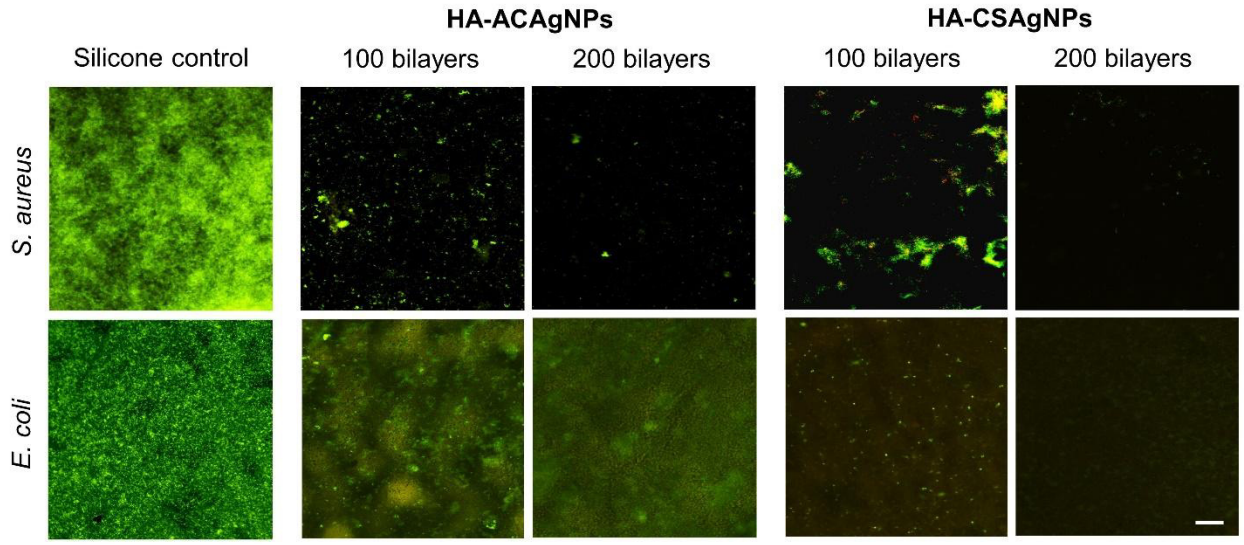

Figure 9. Antibiofilm activity of films. Fluorescence microscopy images (x10 magnification) after Live/Dead staining of *S. aureus* and *E. coli* biofilms on silicone control and on HA-ACAgNPs and HA-CSAgNPs multilayer nanobiocomposites. The scale bar corresponds to 100 μm.

Biocompatibility of the films

AgNPs are among the approved by the U.S. Food and Drug Administration nano-devices for antibacterial applications, e.g. in wounds. However, as human exposure to NPs increased, their nanotoxicity became an emerging and growing concern. Size, shape, and surface chemistry/coating greatly affect the potential risk related to their short- and long-term toxicity.[49,50] The bioavailability of silver ions (Ag^{+}) from AgNPs is considered as a major factor in Ag-mediated toxicity.[51,52] We have previously reported that hybrid nanomaterials comprising metal NPs (ZnO) and antimicrobial biopolymer (namely CS) exhibit very low toxicity coupled to high antimicrobial efficiency.[33] Similarly to the current study, integrating metal NPs with biopolymers with intrinsic antimicrobial properties resulted in reduced cytotoxicity due to the low dissolution rates of the metal from such complexes.[53,54]

Here, the biocompatibility of the developed films was evaluated with human skin fibroblasts and keratinocytes (Fig. 10). After one week of contact, both cell lines were metabolically active with no significant difference in cell viability (above 90 %) observed among the experimental groups. The only exception was for the HA-CSAgNPs membrane with 200 bilayers, which did not induce considerable cell toxicity either, but the cell viability decreased to the still above the acceptable for biomedical applications 80 % after 7 days.

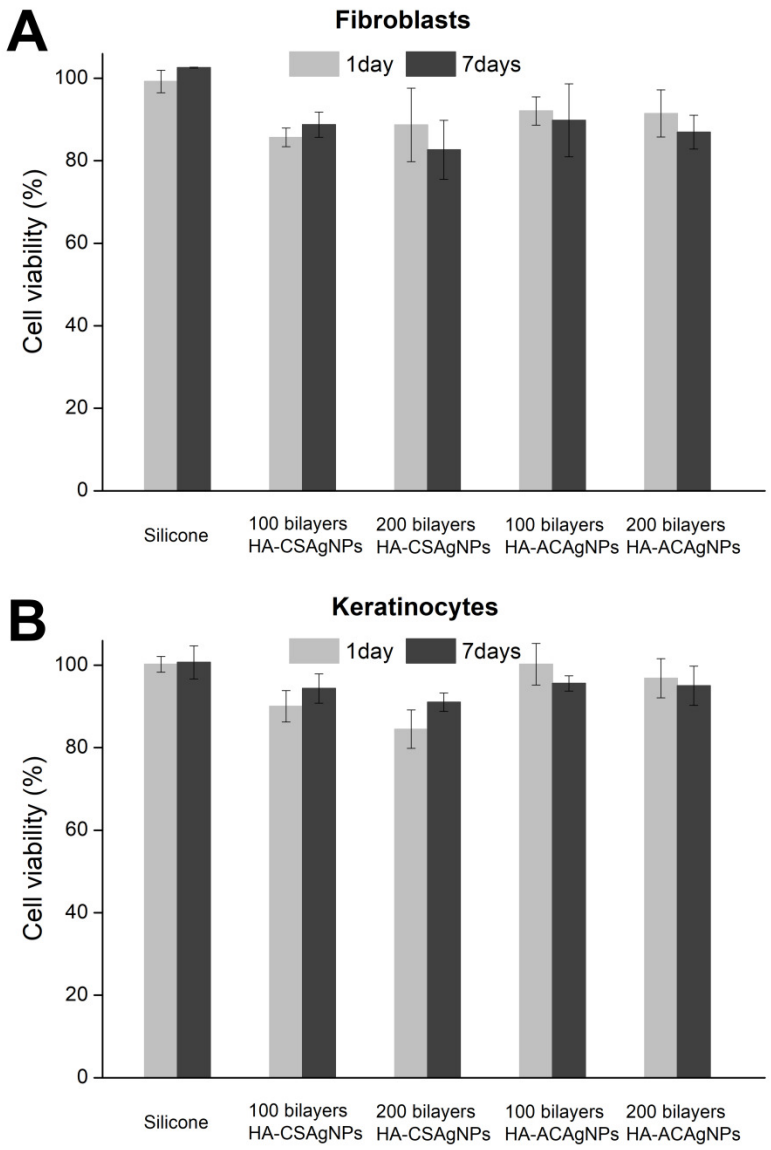

Figure 10. Viability of A) fibroblasts and B) keratinocytes in presence of HA-ACAgNPs and HA-CSAgNPs films of 100 and 200 bilayers.

Conclusions

In this study, the LbL approach was exploited to fabricate freestanding nanobiocomposite films with strong antibacterial and antibiofilm activities against common skin pathogens.

Their antibacterial efficiency is due to the polycation-decorated AgNPs embedded alternately between polyanion HA layers. Prior to their inclusion into the films, the polycationic NPs were synthesized using sonochemistry to complete the overall environmentally friendly approach for the fabrication of functional and safe to human skin cells nanobiocomposite films. The NPs played both i) a structural role to stabilize the final 3D supramolecular nanobiocomposite, and ii) a functional role as a source of antibacterial silver ions. The obtained organic-inorganic multilayer film composites completely inhibited the planktonic growth and biofilm formation by Gram-positive *S. aureus* and Gram-negative *E. coli* pathogens. These features, coupled to their excellent biocompatibility pave the way for their further application as protective dressings for skin injuries to kill bacteria and reduce the risk of infection occurrence.

ASSOCIATED CONTENT

Supporting Information

Topographic AFM images (5 x 5 μm) for 100 LbL films, surface roughness and SEM images with corresponding Ag mapping and EDS spectrum of 200 LbL films. Reduction of *S. aureus* and *E. coli* viability by HA-ACAgNPs and HA-CSAgNPs coatings (10 bilayers) and films comprising 50 bilayers. Inhibition of *S. aureus* and *E. coli* biofilms with the films comprising 100 and 200 bilayers.

AUTHOR INFORMATION *

Corresponding Author

Phone: +34 93 739 85 70; Fax: +34937398225; e-mail: tzanko.tzanov@upc.edu

Author Contributions

The manuscript was written through contributions of all authors. All authors have given approval to the final version of the manuscript.

Notes

The authors declare no competing financial interest

ACKNOWLEDGMENT

This work was supported by the European project PROTECT – "Pre-commercial lines for production of surface nanostructured antimicrobial and anti-biofilm textiles, medical devices and water treatment membranes (H2020 – 720851) and Spanish national project HybridNanoCoat – " Hybrid nanocoatings on indwelling medical devices with enhanced antibacterial and antibiofilm efficiency" (MAT2015-67648-R).

ABBREVIATIONS

AC, aminocellulose; AgNPs, silver nanoparticles; CFU, colony-forming unit; CS, chitosan; *E. coli, Escherichia coli*; HA, hyaluronic acid; LbL, Layer-by-layer; Mw, molecular weight; NB, Nutrient broth; NPs, nanoparticles; O.D., optical density, *S. aureus, Staphylococcus aureus*; SDS, sodium dodecyl sulfate; TSB, tryptic soy broth; US, high-intensity ultrasound.

Conflicts of interest

There are no conflicts to declare.

REFERENCES

(1) Scholz, M. S.; Blanchfield, J. P.; Bloom, L. D.; Coburn, B. H.; Elkington, M.; Fuller, J. D.; Gilbert, M. E.; Muflahi, S. A.; Pernice, M. F.; Rae, S. I.; et al. The Use of Composite Materials in Modern Orthopaedic Medicine and Prosthetic Devices: A Review. *Compos. Sci. Technol.* **2011**, *71* (16), 1791–1803.

(2) Boutrand, J. *Biocompatibility and Performance of Medical Devices*, 1st ed.; Boutrand, J.-P., Ed.; Woodhead Publishing Limited: Philadelphia, 2012.

(3) Paul, D. R.; Robeson, L. M. Polymer Nanotechnology: Nanocomposites. *Polymer (Guildf).* **2008**, *49* (15), 3187–3204.

(4) Hammond, P. T. Building Biomedical Materials Layer-by-Layer. *Mater. Today* **2012**, *15* (5), 196–206.

(5) Ivanova, A.; Ivanova, K.; Hoyo, J.; Heinze, T.; Sanchez-Gomez, S.; Tzanov, T. Layer-By-Layer Decorated Nanoparticles with Tunable Antibacterial and Antibiofilm Properties against Both Gram-Positive and Gram-Negative Bacteria. *ACS Appl. Mater. Interfaces* **2018**, *10* (4), 3314–3323.

(6) Schneider, G.; Decher, G. From Functional Core/Shell Nanoparticles Prepared via Layer-by-Layer Deposition to Empty Nanospheres. *Nano Lett.* **2004**, *4* (10), 1833–1839.

(7) Francesko, A.; Fernandes, M. M.; Ivanova, K.; Amorim, S.; Reis, R. L.; Pashkuleva, I.; Mendoza, E.; Pfeifer, A.; Heinze, T.; Tzanov, T. Bacteria-Responsive Multilayer Coatings

Comprising Polycationic Nanospheres for Bacteria Biofilm Prevention on Urinary Catheters. *Acta Biomater.* **2016**, *33*, 203–212.

(8) Zhuk, I.; Jariwala, F.; Attygalle, A. B.; Wu, Y.; Libera, M. R.; Sukhishvili, S. A. Self-Defensive Layer-by-Layer Films with Bacteria-Triggered Antibiotic Release. *ACS Nano* **2014**, *8* (8), 7733–7745.

(9) Mallwitz, F.; Laschewsky, A. Direct Access to Stable, Freestanding Polymer Membranes by Layer-by-Layer Assembly of Polyelectrolytes. *Adv. Mater.* **2005**, *17* (10), 1296–1299.

(10) Correia, C. R.; Reis, R. L.; Mano, J. F. Multilayered Hierarchical Capsules Providing Cell Adhesion Sites. *Biomacromolecules* **2013**, *14* (3), 743–751.

(11) Francesko, A.; Soares da Costa, D.; Lisboa, P.; Reis, R. L.; Pashkuleva, I.; Tzanov, T. GAGs-Thiolated Chitosan Assemblies for Chronic Wounds Treatment: Control of Enzyme Activity and Cell Attachment. *J. Mater. Chem.* **2012**, *22* (37), 19438–19446.

(12) Jiang, C.; Tsukruk, V. V. Freestanding Nanostructures via Layer-by-Layer Assembly. *Adv. Mater.* **2006**, *18* (7), 829–840.

(13) Larkin, A. L.; Davis, R. M.; Rajagopalan, P. Biocompatible, Detachable, and Free-Standing Polyelectrolyte Multilayer Films. *Biomacromolecules* **2010**, *11* (10), 2788–2796.

(14) Silva, J. M.; Duarte, A. R. C.; Caridade, S. G.; Picart, C.; Reis, R. L.; Mano, J. F. Tailored Freestanding Multilayered Membranes Based on Chitosan and Alginate. *Biomacromolecules* **2014**, *15* (10), 3817–3826.

(15) Silva, J. M.; Georgi, N.; Costa, R.; Sher, P.; Reis, R. L.; van Blitterswijk, C. A.; Karperien, M.; Mano, J. F. Nanostructured 3D Constructs Based on Chitosan and Chondroitin Sulphate Multilayers for Cartilage Tissue Engineering. *PLoS One* **2013**, *8* (2).

(16) Sher, P.; Custódio, C. A.; Mano, J. F. Layer-By-Layer Technique for Producing Porous

Nanostructured 3D Constructs Using Moldable Freeform Assembly of Spherical Templates. *Small* **2010**, *6* (23), 2644–2648.

(17) Xu, Q.; Zheng, Z.; Wang, B.; Mao, H.; Yan, F. Zinc Ion Coordinated Poly(Ionic Liquid) Antimicrobial Membranes for Wound Healing. *ACS Appl. Mater. Interfaces* **2017**, *9* (17), 14656–14664.

(18) Go, D. P.; Hung, A.; Gras, S. L.; O'Connor, A. J. Use of a Short Peptide as a Building Block in the Layer-by-Layer Assembly of Biomolecules on Polymeric Surfaces. *J. Phys. Chem. B* **2012**, *116* (3), 1120–1133.

(19) Borges, J.; Sousa, M. P.; Cinar, G.; Caridade, S. G.; Guler, M. O.; Mano, J. F. Nanoengineering Hybrid Supramolecular Multilayered Biomaterials Using Polysaccharides and Self-Assembling Peptide Amphiphiles. *Adv. Funct. Mater.* **2017**, *27* (17).

(20) Buck, M. E.; Lynn, D. M. Free-Standing and Reactive Thin Films Fabricated by Covalent Layer-by-Layer Assembly and Subsequent Lift-off of Azlactone-Containing Polymer Multilayers. *Langmuir* **2010**, *26* (20), 16134–16140.

(21) Madaghiele, M.; Sannino, A.; Ambrosio, L.; Demitri, C. Polymeric Hydrogels for Burn Wound Care: Advanced Skin Wound Dressings and Regenerative Templates. *Burn. Trauma* **2014**, *2* (4), 153.

(22) Sussman, G.; Golding, M. Skin Tears: Should the Emphasis Be Only Their Management? *Wound Pract. Res.* **2011**, *19* (2).

(23) Reidy, B.; Haase, A.; Luch, A.; Dawson, K. A.; Lynch, I. Mechanisms of Silver Nanoparticle Release, Transformation and Toxicity: A Critical Review of Current Knowledge and Recommendations for Future Studies and Applications. *Materials (Basel).*

2013, *6*, 2295–2350.

(24) Sportelli, M. C.; Picca, R. A.; Cioffi, N. Recent Advances in the Synthesis and Characterization of Nano-Antimicrobials. *TrAC Trends Anal. Chem.* **2016**, *84*, *Part A*, 131–138.

(25) Le Ouay, B.; Stellacci, F. Antibacterial Activity of Silver Nanoparticles: A Surface Science Insight. *Nano Today* **2015**, *10* (3), 339–354.

(26) Vazquez-Muñoz, R.; Borrego, B.; Juárez-Moreno, K.; García-García, M.; Mota Morales, J. D.; Bogdanchikova, N.; Huerta-Saquero, A. Toxicity of Silver Nanoparticles in Biological Systems: Does the Complexity of Biological Systems Matter? *Toxicol. Lett.* **2017**, *276* (May), 11–20.

(27) Francesko, A.; Cano Fossas, M.; Petkova, P.; Fernandes, M. M.; Mendoza, E.; Tzanov, T. Sonochemical Synthesis and Stabilization of Concentrated Antimicrobial Silver-Chitosan Nanoparticle Dispersions. *J. Appl. Polym. Sci.* **2017**, *134* (30), 1–8.

(28) Francesko, A.; Blandón, L.; Vázquez, M.; Petkova, P.; Morató, J.; Pfeifer, A.; Heinze, T.; Mendoza, E.; Tzanov, T. Enzymatic Functionalization of Cork Surface with Antimicrobial Hybrid Biopolymer/Silver Nanoparticles. *ACS Appl. Mater. Interfaces* **2015**, *7* (18), 9792–9799.

(29) Petkovšek, Ž.; Eleršič, K.; Gubina, M.; Žgur-Bertok, D.; Erjavec, M. S. Virulence Potential of Escherichia Coli Isolates from Skin and Soft Tissue Infections. *J. Clin. Microbiol.* **2009**, *47* (6), 1811–1817.

(30) Fung, H. B.; Chang, J. Y.; Kuczynski, S. A Practical Guide to the Treatment of Complicated Skin and Soft Tissue Infections. *Drugs* **2003**, *63* (14), 1459–1480.

(31) Rahn, K.; Diamantoglou, M.; Klemm, D.; Berghmans, H.; Heinze, T. Homogeneous

Synthesis of Cellulose P-Toluenesulfonates in N , N-Dimethylacetamidel LiCl Solvent System. *Die Angew. Makromol. Chemie* **1996**, *238* (1), 143–163.

(32) Ivanova, K.; Fernandes, M. M.; Mendoza, E.; Tzanov, T. Enzyme Multilayer Coatings Inhibit Pseudomonas Aeruginosa Biofilm Formation on Urinary Catheters. *Appl. Microbiol. Biotechnol.* **2015**, *99* (10), 4373–4385.

(33) Petkova, P.; Francesko, A.; Fernandes, M. M.; Mendoza, E.; Perelshtein, I.; Gedanken, A.; Tzanov, T. Sonochemical Coating of Textiles with Hybrid ZnO/Chitosan Antimicrobial Nanoparticles. *ACS Appl. Mater. Interfaces* **2014**, *6* (2), 1164–1172.

(34) Wang, Q. Z.; Chen, X. G.; Liu, N.; Wang, S. X.; Liu, C. S.; Meng, X. H.; Liu, C. G. Protonation Constants of Chitosan with Different Molecular Weight and Degree of Deacetylation. *Carbohydr. Polym.* **2006**, *65* (2), 194–201.

(35) Zemljič, L. F.; Čakara, D.; Michaelis, N.; Heinze, T.; Kleinschek, K. S. Protonation Behavior of 6-Deoxy-6-(2-Aminoethyl)Amino Cellulose: A Potentiometric Titration Study. *Cellulose* **2011**, *18* (1), 33–43.

(36) Haxaire, K.; Maréchal, Y.; Milas, M.; Rinaudo, M. Hydration of Polysaccharide Hyaluronan Observed by IR Spectrometry. I. Preliminary Experiments and Band Assignments. *Biopolym. - Biospectroscopy Sect.* **2003**, *72* (1), 10–20.

(37) Richert, L.; Lavalle, P.; Payan, E.; Shu, X. Z.; Prestwich, G. D.; Stoltz, J.-F.; Schaaf, P.; Voegel, J.-C.; Picart, C. Layer by Layer Buildup of Polysaccharide Films: Physical Chemistry and Cellular Adhesion Aspects. *Langmuir* **2003**, *20* (2), 448–458.

(38) Slavin, Y. N.; Asnis, J.; Häfeli, U. O.; Bach, H. Metal Nanoparticles: Understanding the Mechanisms behind Antibacterial Activity. *J. Nanobiotechnology* **2017**, *15* (1), 1–20.

(39) Fernandes, M. M.; Francesko, A.; Torrent-Burgués, A.; Carrión-Fité, F. J.; Heinze, T.;

Tzanov, T. Sonochemically Processed Cationic Nanocapsules: Efficient Antimicrobials with Membrane Disturbing Capacity. *Biomacromolecules* **2014**, *15* (4), 1365–1374.

(40) Macdonald, T. J.; Wu, K.; Sehmi, S. K.; Noimark, S.; Peveler, W. J.; du Toit, H.; Voelcker, N. H.; Allan, E.; MacRobert, A. J.; Gavriilidis, A.; et al. Thiol-Capped Gold Nanoparticles Swell-Encapsulated into Polyurethane as Powerful Antibacterial Surfaces Under Dark and Light Conditions. *Sci. Rep.* **2016**, *6* (1), 39272.

(41) Tang, H.; Cao, T.; Liang, X.; Wang, A.; Salley, S. O.; McAllister, J.; Ng, K. Y. S. Influence of Silicone Surface Roughness and Hydrophobicity on Adhesion and Colonization of Staphylococcus Epidermidis. *J. Biomed. Mater. Res. - Part A* **2009**, *88* (2), 454–463.

(42) Braem, A.; Van Mellaert, L.; Mattheys, T.; Hofmans, D.; De Waelheyns, E.; Geris, L.; Anne, J.; Schrooten, J.; Vleugels, J. Staphylococcal Biofilm Growth on Smooth and Porous Titanium Coatings for Biomedical Applications. *J. Biomed. Mater. Res. - Part A* **2014**, *102* (1), 215–224.

(43) Meiron, T. S.; Saguy, I. S. Adhesion Modeling on Rough Low Linear Density Polyethylene. *J. Food Sci.* **2007**, *72* (9), 485–491.

(44) Cunliffe, D.; Smart, C. A.; Alexander, C.; Vulfson, E. N. Bacterial Adhesion at Synthetic Surfaces. *Appl. Environ. Microbiol.* **1999**, *65* (11), 4995–5002.

(45) Scardino, A. J.; de Nys, R. Mini Review: Biomimetic Models and Bioinspired Surfaces for Fouling Control. *Biofouling* **2011**, *27* (1), 73–86.

(46) Khoo, X.; Grinstaff, M. W. Novel Infection-Resistant Surface Coatings: A Bioengineering Approach. *MRS Bull.* **2011**, *36* (5), 357–366.

(47) Xue, Y.; Xiao, H.; Zhang, Y. Antimicrobial Polymeric Materials with Quaternary

Ammonium and Phosphonium Salts. *Int. J. Mol. Sci.* **2015**, *16* (2), 3626–3655.

(48) Mathews, S.; Hans, M.; Mücklich, F.; Solioz, M. Contact Killing of Bacteria on Copper Is Suppressed If Bacterial-Metal Contact Is Prevented and Is Induced on Iron by Copper Ions. *Appl. Environ. Microbiol.* **2013**, *79* (8), 2605–2611.

(49) Carlson, C.; Hussein, S. M.; Schrand, A. M.; Braydich-Stolle, L. K.; Hess, K. L.; Jones, R. L.; Schlager, J. J. Unique Cellular Interaction of Silver Nanoparticles: Size-Dependent Generation of Reactive Oxygen Species. *J. Phys. Chem. B* **2008**, *112* (43), 13608–13619.

(50) El Badawy, A. M.; Silva, R. G.; Morris, B.; Scheckel, K. G.; Suidan, M. T.; Tolaymat, T. M. Surface Charge-Dependent Toxicity of Silver Nanoparticles. *Environ. Sci. Technol.* **2011**, *45* (1), 283–287.

(51) Lubick, N. Nanosilver Toxicity: Ions, Nanoparticles—or Both? *Environ. Sci. Technol.* **2008**, *42* (23), 8617.

(52) Kim, S.; Choi, J. E.; Choi, J.; Chung, K.-H.; Park, K.; Yi, J.; Ryu, D.-Y. Oxidative Stress-Dependent Toxicity of Silver Nanoparticles in Human Hepatoma Cells. *Toxicol. Vitr.* **2009**, *23* (6), 1076–1084.

(53) Krishnaveni, R.; Thambidurai, S. Industrial Method of Cotton Fabric Finishing with Chitosan–ZnO Composite for Anti-Bacterial and Thermal Stability. *Ind. Crops Prod.* **2013**, *47*, 160–167.

(54) Li, L.-H.; Deng, J.-C.; Deng, H.-R.; Liu, Z.-L.; Li, X.-L. Preparation, Characterization and Antimicrobial Activities of Chitosan/Ag/ZnO Blend Films. *Chem. Eng. J.* **2010**, *160* (1), 378–382.

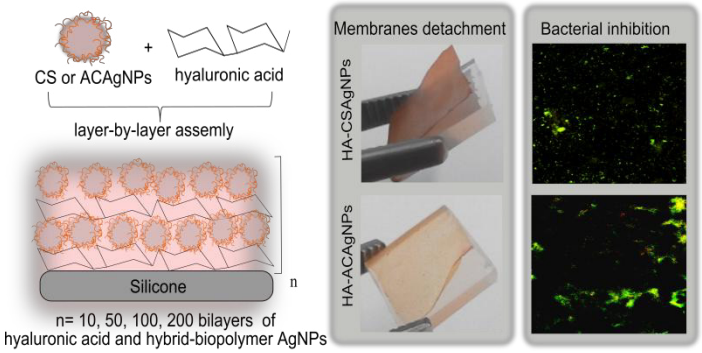
CS or ACAgNPs
+
hyaluronic acid
layer-by-layer assemly
Silicone
n
n= 10, 50, 100, 200 bilayers of
hyaluronic acid and hybrid-biopolymer AgNPs
Membranes detachment
Bacterial inhibition
HA-CSAgNPs
HA-ACAgNPs

1